M-shaped Under-Bridge Feeding Method For A Low-Profile Dual-Band Dual-Polarized Antenna-on-Package In The 6G Upper-mid Band

Jeongtaek Oh, Hyunjin Kim, Sucheoul Kim, Jaehyun Choi, Jihun Ha and Jungsuek Oh

***Abstract*—A 2×4 dual-feed antenna-on-package (AoP) for 6G upper-midband supports high-power and dual-polarization, with a compact structure enabling potential use in smartphones and dense MIMO base stations. The dual-feed antenna element is designed considering dual-linear polarization and dual-band operation. Consequently, the proposed antenna can provide dual-band, achieving an −6 dB impedance bandwidth of 32.3% (9.77 GHz–13.45 GHz), port-to-port isolation higher than −15 dB, and the envelope correlation coefficient lesser than 0.02. The 2×4 antenna array for a MIMO antenna is fabricated for the evaluation of radiation characteristics. The proposed antennas are measured and verified by vertical probing system. Each element was measured with −6 dB impedance bandwidth of over 6.83% in low-band and 4.9% in high-band. The measured gain of boresight is achieved to 6.45 dBi at 10.25 GHz, and 6.7 dBi at 12.7 GHz, and the measured ECCs are all less than 0.04 in the dual bandwidth.**

***Index Terms*—6G Upper-mid band, Antenna-on-package, MIMO antenna, Mobile antenna**

I. Introduction

UPPER mid-band has recently emerged as a candidate frequency range for 6G mobile communication. With delays in the commercialization of 5G systems, there has been a shift toward lowering communication frequencies, allowing for more flexible use. The following new bands were proposed for wireless broadband use, 7.025 GHz–7.125 GHz, 10 GHz–10.5 GHz, and 12.7 GHz–13.25 GHz (the upper 12 GHz band) [1]–[3]. Among these, 6G upper-mid technology is a promising candidate for implementing a high channel capacity, healthcare, and other applications. The coverage of upper-midband could be less limited by increased oxygen absorption, path loss, and blockages, which is expected to improve coverage from the perspective of mobile devices. Antennas composed of multiple layers, such as antenna-on-package (AoP), antenna-in-package (AiP), and antenna-in-display (AiD) for 5G systems, have been developed with each layer thinner than 100 μm ($< 0.01\ \lambda$ at 28 GHz) and advanced technologies to enhance line width resolution to support high-frequency operation at millimeter-wave (mm-Wave) and sub-THz bands [4]–[11]. This has led to the development of extremely low-profile antennas around 1 mm of total thickness, and commercial mobile devices now demand 6G antennas with high radiation performance within the same thickness constraints [13], [14]. However, 6G AoP modules must support multi-input multi-output (MIMO) systems to ensure reliable communication even within a compact form factor, and they are required to achieve dual polarization to enhance reception capacity performance [14]. MIMO antenna technologies for mobile devices were designed for a single band of 6.425 GHz–8.4 GHz, which has particular challenges in achieving dual bandwidth [13], [15].

Here, a novel M-shaped under-bridge (MUB) feeding structure is proposed for a dual-band, dual-linearly polarized compact patch antenna, targeting impedance-matching 6G MIMO AoP module applications. The AoP consists of multilayer PCBs as in [5], however reduced thickness makes it difficult to maintain the reflection coefficient bandwidth in the upper-midband. By adopting MUB indirect feeding, the proposed antenna overcomes bandwidth limitations and improves reflection coefficient and port isolation, which is further validated through thorough evaluation of the fabricated AoP module.

The rest of the letter is overviewed as follows. In Section II, the structure of the proposed antenna-on-package is described, and the principles of MUB feeding method are discussed in Section III. Section IV presents the verified results with measurements. Finally, Section V concludes this letter.

II. Proposed Antenna-on-Package Design

A. 3D Structure of the proposed AoP module

Fig. 1 illustrates the proposed AoP module for MIMO upper-midband mobile applications. A 2×4 antenna array is proposed to consist of 16 ports, which is designed for each element to operate with two feeding ports to enable dual-polarization as shown in Fig. 1 (a). The single element of the proposed antenna consists of a circular patch resonating at the low band, and a ring patch segmented by four sectors designed to resonate together with it at the high band as shown in Fig. 1 (b). Sub-wavelength-sized dummy patterns were placed below the radiator to meet the copper balance requirement of the multilayer stack-up process. These patterns were strategically designed and arranged only around the circular resonant patch to minimize their impact on the resonant patch and the feeding structure.

This work was supported and funded in part by LG Innotek; and in part by the Institute for Information communications Technology Promotion (IITP) grant funded by the Korea government (MSIT) (RS-2024-00395366). (Corresponding author: Jungsuek Oh.)

Jeongtaek Oh and Jungsuek Oh are with the Department of Electrical and Computer Engineering, Institute of New Media and Communications(INMC), Seoul National University, Seoul 08826, South Korea (e-mail: iwalife@snu.ac.kr; jungsuek@snu.ac.kr). Sucheoul Kim, Chanwoo Yang, Jaehyun Choi and Jihun Ha are with LG Innotek, Seoul 07795, South Korea (e-mail: charles.kim@lginnotek.com; eddie0625@lginnotek.com; jaehyunchoi@lginnotek.com; jihun.ha@lginnotek.com).

This article has been accepted for publication in IEEE Antennas and Wireless Propagation Letters. This is the author's version which has not been fully edited and content may change prior to final publication. Citation information: DOI 10.1109/LAWP.2025.3585144

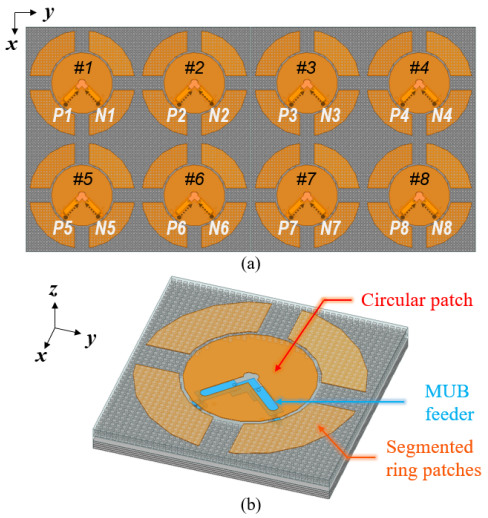

Fig. 1. Proposed AiP module for mobile applications. (a) Top view of the proposed 2 × 4 antenna array. (b) 3-D structure of a single element.

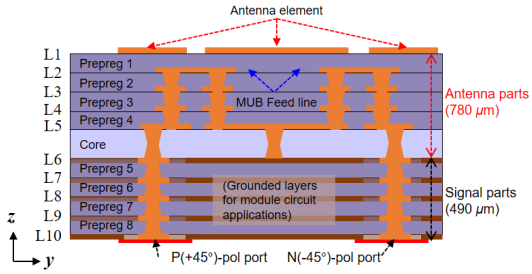

Fig. 2. Layer stack-up of the proposed AoP module: 10 layers.

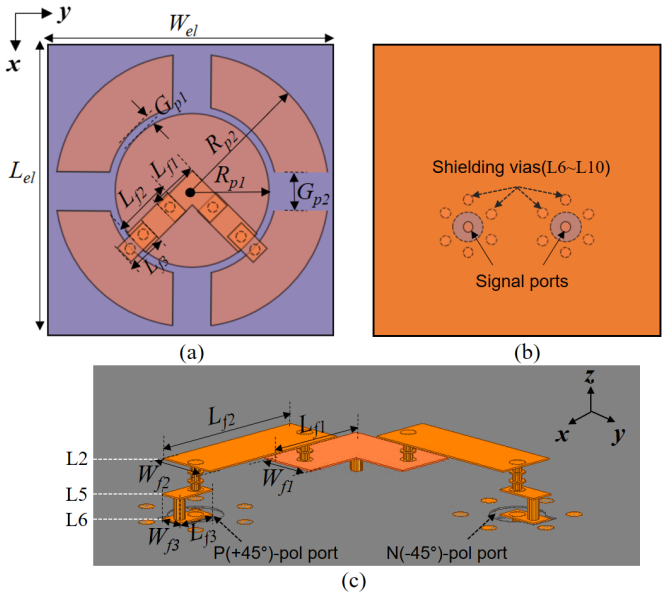

Fig. 3. (a) The top view, (b) The bottom view of proposed antenna, and (c) the detailed description of the MUB feeding structure.

TABLE I
OPTIMIZED DIMENSIONS OF THE SINGLE ANTENNA IN FIG. 3 (UNIT: MILLIMETER).

Parameter	Value	Parameter	Value
L_{el}	12.5 (0.5 λ_0)	W_{el}	12.5 (0.5 λ_0)
L_{f1}	0.8	W_{f1}	0.8
L_{f2}	2.2	W_{f2}	0.8
L_{f3}	0.58	W_{f3}	0.3
R_{p1}	3.4	G_{p1}	0.2
R_{p1}	5.9	G_{p2}	1.6

B. Multilayer structure of AoP

The antenna is mounted in a multi-layer sutructure as shown in Fig. 2, using substrates above the 300μm-thick core (layer 3). The prepreg substrate has a permittivity value (ε_r) of 3.53, loss tangent (tan δ) value of 0.004 and a thickness of 100 μm. Each metal layer is composed of 18 μm. The practical antenna mounting space in a multi-layer structure utilizes the substrates above the core (layer 1–layer 5), with the core substrate (layer 3) having a thickness of 300 μm. Therefore, layer 6 serves as the main ground (GND) plane, and the substrates below are designed as circular ports for measurement purposes via drills. The proposed antenna is designed with this configuration to achieve dual-band operation within the upper-midband bandwidth, satisfying the reflection coefficient criterion below −6 dB in the antenna section, while maintaining the ignorable loss of compact signal line in the signal section. It also offers a wide degree of design freedom and enables high antenna performance.

C. M-shaped Under-Bridge Indirect Matching Structure

The M-shaped under-bridge (MUB) feeding structure proposed in this paper is designed to secure bandwidth for a dual-band patch antenna. This requires the prior design of a radiating element capable of dual resonance. One effective method for achieving dual resonance in patch antennas involves surrounding the main patch with a parasitic patch. Fig. 3 (a) shows the top view of the antenna,consisting of a circular patch with a surrounding ring patch divided into four sectors. The MUB structure enables slant polarization and wideband matching by connecting orthogonal P- and N-port L-probes. The microstrip line on layer 5 (L5) is connected to each L-probe form through vias and is grounded through a central via. To support flip-chip type integration of the AoP module, the ground layer (L10) supports flip-chip integration with shielded cylindrical ports as shown in 3 (b). The MUB structure not only preserves strong coupling to the circular patch but also maximizes isolation between the P-and N-port via the central bridge, as shown in Fig. 3(c). This is achieved by parameric study of the bridge design parameter L_{f1}, W_{f1}.

III. PRINCIPLE OF MUB DESIGN

The Z-parameters and S-parameters for the L-probe feeding structure are compared considering variations in the L_{f2} parameter, as shown in Fig. 4. According to Fig. 4(a), the radiating patch is capable of supporting dual-band radiation. However, as shown in Fig. 4(b), the mutual coupling between the two orthogonal feeding ports remains significant, resulting in a limited isolation level of approximately −12.4 dB. This level of interference poses a challenge in realizing effective port decoupling, thereby restricting the overall performance of the antenna system.

This article has been accepted for publication in IEEE Antennas and Wireless Propagation Letters. This is the author's version which has not been fully edited and content may change prior to final publication. Citation information: DOI 10.1109/LAWP.2025.3585144

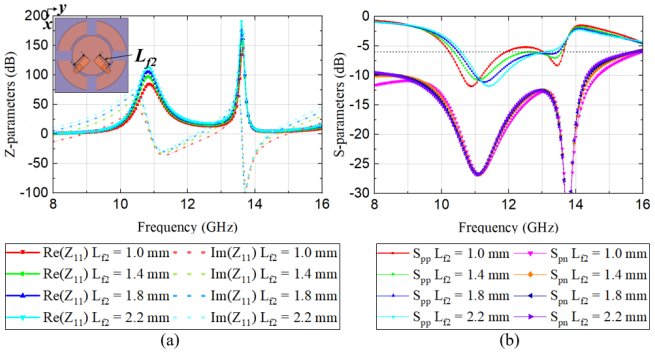

Fig. 4. Proposed antenna with L-probe feeding structure instead of MUB feeding structure. (a) Z-paramters, and (b) S-parameters along the variation of L_{f2}.

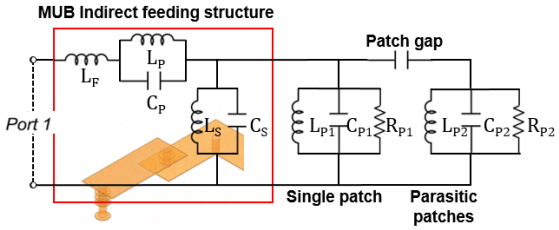

Fig. 5. The equivalent circuit model of MUB feeding structure. The component values are: $L_F = 0.64$, nH, $L_P = 0.28$, nH, $C_P = 1.04$ pF, $L_S = 0.64$ nH, $C_S = 0.24$ pF.

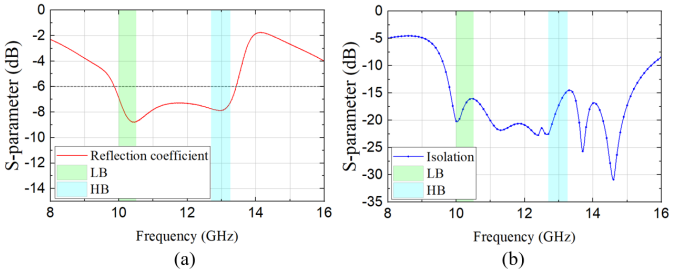

Fig. 6. Reflection coefficient and isolation of the proposed antenna with an optimized MUB feeding structure.

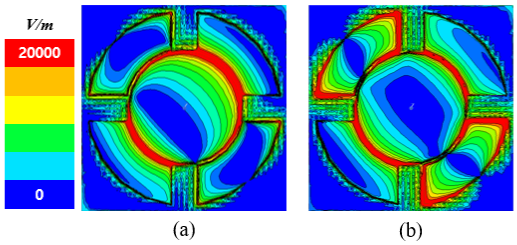

Fig. 7. Electric field distribution of the proposed antenna on the top layer at (a) 10 GHz, and (b) 12.7 GHz when P-port is ON.

To address this limitation, the feeding structure is interpreted as a dual-resonant impedance-matching network comprising both series and parallel RLC elements. This model is intended to synthesize an impedance matching over two distinct frequency bands. The L-probe coupled-feeder can be equivalently represented by a series component. The L-probe coupled-feeder can be equivalently represented by a series component L_F (corresponding to the vertical via from the port), and parallel components L_P and C_P (representing the microstrip line section isolated from the radiating patch). However, the conventional L-probe feeder alone is insufficient in effectively suppressing the coupling between the orthogonally oriented ports. Therefore, the proposed MUB structure is introduced to incorporate a bridge layer that serves as an additional mechanism for enhancing port-to-port isolation. This bridge layer can be equivalently modeled using a shunt components L_S and C_S, which dominate the isolation behavior between the two resonant paths. Fig. 5 illustrates the equivalent circuit model of the proposed MUB feeding structure, which represents the coupling characteristics between the radiating patch and the MUB-based feeding mechanism.

The MUB feeding structure controls the isolation between the two ports while achieving reflection coefficients better than −6 dB across the operating band, corresponding to the widely adopted 3:1 VSWR criterion for mobile antennas. The optimized bandwidth is 9.77 GHz–13.25 GHz, and the isolation level is under −15 dB over the bandwidth as shown in Fig. 6. Fig. 7 shows that the electric field is distributed on the main patch at 10 GHz, and is strongly distributed on the parasitic patches together at 12.7 GHz with when it is optimized with the MUB feeding structure. Fig. 8 shows the 3-D far-field radiation pattern of the proposed antenna for dual frequency, respectively.

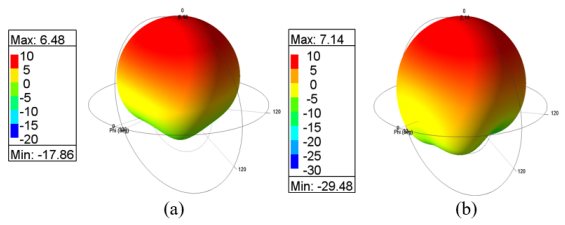

Fig. 8. 3D far-field radiation pattern of realized gain at (a) 10 GHz, and (b) 12.7 GHz when P-port is ON.

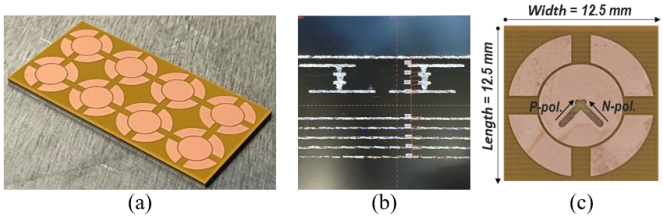

Fig. 9. (a) The fabricated 2×4 antenna array. (b) X-ray photograph of the side cross-section of the fabricated sample. (c) Top view of the radiating patch with an added slot structure.

IV. Fabrication and Measurement

The Fig. 9 (a) shows the fabricated sample of the proposed antenna. The thickness of the fabricated antenna is precisely measured through a cross-section cut as shown in Fig. 9 (b), revealing a change in the thickness of the antenna substrate. Upper substrate of the antenna part became thinner by 12.5 μm each. Consequently, the spacing between the metal layers (L1

This article has been accepted for publication in IEEE Antennas and Wireless Propagation Letters. This is the author's version which has not been fully edited and content may change prior to final publication. Citation information: DOI 10.1109/LAWP.2025.3585144

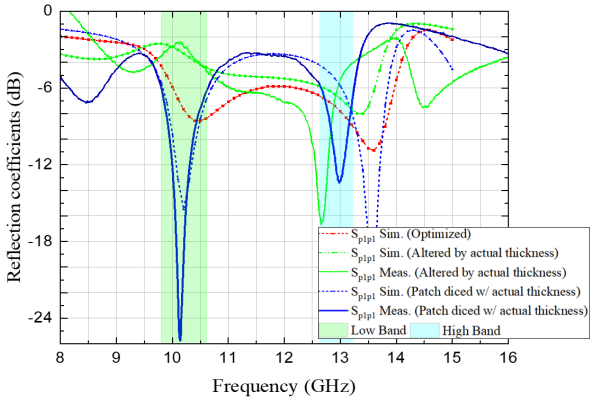

Fig. 10. Compared reflection coefficients of the fabricated samples.

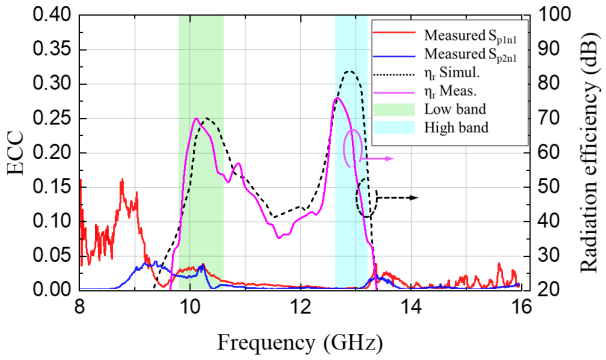

Fig. 11. Envelope correlation coefficient (ECC) and radiation efficiency of a single antenna element along frequency, based on measured $S_{p_1N_1}$, $S_{P_2N_1}$, and simulated/measured efficiency.

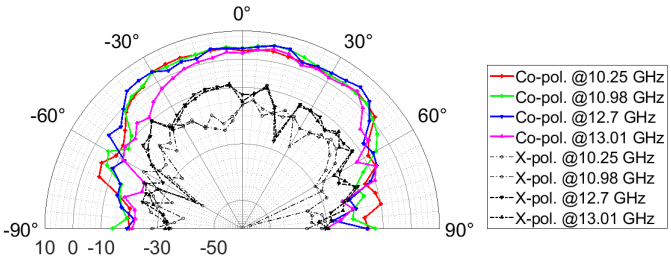

Fig. 12. Far-field radiation patterns of the realized gain at +45° plane, when P1-port of the proposed antenna is ON.

and L2) is significantly influenced by the coupling between the feed structure and the radiating patches.

The fabricated sample was measured using a vertically mountable measurement (VMM) setup with a vector network analyzer (VNA) and 650μm-pitch GSG probes. Calibration and measurement of the modules were carried out on a RO-HACELL foam. The bandwidth of the fabricated sample was altered due to changes in the actual thickness. The thickness of each substrate layer is measured using the cross-section of the X-ray image as shown in Fig. 9 (b). The measured reflection coefficients are analyzed by comparing the modified substrate thickness into the simulation, as presented in Fig. 10. It is presumed that the substrate thickness variation influenced the coupling (L_P, C_P) of the MUB feeding structure, as illustrated by the equivalent circuit in Fig. 5. Slot structures are added to the resonant patch to modify the coupling between the resonant patch and the MUB feeding structure as shown in Fig. 9 (c). This slot is a defected structure designed along the direction parallel to the MUB feeding line within the patch pattern, with dimensions of 3.1 mm × 0.53 mm. Finally, the measured results of the modified sample closely resemble the simulation results, with the measured reflection coefficient bandwidth under −6 dB to be 9.81 GHz–10.63 GHz, and 12.65 GHz–13.24 GHz as shown in Fig. 10, which corresponds to the simulation results. The ECC measurement results were obtained by calculating far-field radiation patterns of a single element. As shown in Fig. 11, for the dual-bandwidth operation, the ECC values remain below 0.03, confirming the uncorrelated nature between the ports. The proposed antenna exhibits broad radiation characteristics with realized gains of 6.45 dBi and 6.7 dBi, and radiation efficiencies of 85.9% and 89.14% at 10.25 GHz and 12.7 GHz, respectively. The far-field radiation pattern of the proposed antenna is measured as shown in Fig. 12.

V. Conclusion

A novel dual-feed AoP module has been proposed for 6G upper-midband applications, featuring dual-linear polarization and dual-band operation within a compact multilayer PCB. The introduction of an M-shaped under-bridge (MUB) feeding structure is a key innovation, enabling improved impedance matching and wideband performance while maintaining a low-profile and space-efficient design. The fabricated 2 × 4 AoP array achieves impedance bandwidths of −6 dB of 9.81–10.63 GHz and 12.65–13.24 GHz, with ECC values below 0.03 across both bands, indicating proper isolation. These findings demonstrate that the proposed MUB-enabled AoP architecture offers strong potential for integration into high-performance and space-constrained MIMO systems in next-generation mobile devices.

TABLE II
Comparison of State-of-Art Upper-Midband Antennas.

Ref.	Bandwidth	Arrays	Number of Ports	Size ($W \times L \times t$)**	ECC
[5]	26–31, 37–40	1×4	8	$0.49\lambda_0 \times 0.49\lambda_0 \times 0.089\lambda_0$	N.A.
[12]	7.025–8.4*	2×2	16	$0.8\lambda_0 \times 0.8\lambda_0 \times 0.026\lambda_0$	< 0.05
[13]	7.025–8.4*	2×2	16	$0.5\lambda_0 \times 0.5\lambda_0 \times 0.026\lambda_0$	< 0.005
[14]	6.4–8.6	1×2	8	$0.59\lambda_0 \times 0.59\lambda_0 \times 0.025\lambda_0$	< 0.02
This work	9.81–10.63, 12.65–13.24*	2×4	16	$0.5\lambda_0 \times 0.5\lambda_0 \times 0.029\lambda_0$	< 0.03

∗ The -6 dB matching criterion is commonly adopted for evaluating the effectiveness of mobile antennas.
∗∗ The size is based on a single element.

REFERENCES

[1] [Online] Available: https://www.itu.int/md/meetingdoc.asp?lang=en&parent=R23-WRC23-C&source=United%20States%20of%20America

[2] S. Sambhwani et al., "Transitioning to 6G Part 1: Radio Technologies," *IEEE Wireless Communications*, vol. 29, no. 1, pp. 6–8, 2022.

[3] K. Lee, J. Kim, E. W. Jin, and K. S. Kim, "Extreme Massive MIMO for Upper-Mid Band 6G Communications," *in 2022 13th International Conference on Information and Communication Technology Convergence (ICTC)*, pp. 997–999, Oct. 2022.

[4] J. Seo et al., "Miniaturized Dual-Band Broadside/Endfire Antenna-in-Package for 5G Smartphone," *IEEE Transactions on Antennas and Propagation*, vol. 69, no. 12, pp. 8100–8114, 2021.

[5] G. Kim, D. Kim, K. Lim, C. Yang, C. You, and S. Kim, "Dual-Band and Dual-Polarized Rhombic Patch Antenna Array for 5G mmWave RF Front End Antenna-in-Package Module," *IEEE Antennas and Wireless Propagation Letters*, vol. 23, no. 7, pp. 2120–2124, 2024.

[6] X. Xia et al., "Millimeter-Wave Phased Array Antenna Integrated With the Industry Design in 5G/B5G Smartphones," *IEEE Transactions on Antennas and Propagation*, vol. 71, no. 2, pp. 1883–1888, 2023.

[7] B. Kim, J. Jung, S. Yun, H. Kim and J. Oh, "Heterogeneous Metasurface Empowering Proximate High-Permittivity Ceramic Cover for a 5G Dual-Band Millimeter-Wave Smartphone," *IEEE Transactions on Antennas and Propagation*, vol. 72, no. 5, pp. 4086–4094, 2024.

[8] M. R. Al-Amin, R. S. Malfajani, E. Baladi, and M. S. Sharawi, "Connected Antenna Arrays With Beamsteering Capability for On-Package Millimetre-Wave Applications," *IEEE Open Journal of Antennas and Propagation*, vol. 5, no. 2, pp. 414–429, 2024.

[9] T. Ding, M. Wang, A. Kou, C. Z. Han, and J. Xiao, "High-Gain Circularly Polarized Array Antenna Based on High-Order Mode ESIC for 5G Millimeter-Wave Application," *IEEE Antennas and Wireless Propagation Letters*, vol. 23, no. 10, pp. 3063–3067, 2024.

[10] J. Oh, B. Kim, S. Yoon, K. Kim, E. J. Sung and J. Oh, "High-Gain Millimeter-Wave Antenna-in-Display Using Non-Optical Space for 5G Smartphones," *IEEE Transactions on Antennas and Propagation*, vol. 71, no. 2, pp. 1458–1468, Feb. 2023.

[11] H. Kim, J. Jung, W. Lee, S. Nam, and J. Oh, "D-Band 4×4 Multi-Feed Array Antenna-in-Package for High-Power Combining and Polarization Synthesis," *IEEE Access*, vol. 11, pp. 144006–144016, 2023.

[12] J. Choi, W. Park, S. Kim, C. You, and K. L. Wong, "Low-Profile High-Density MIMO Antenna Module Incorporating a 16-Port Configuration for 6G Upper Mid-Band Mobile Application," *in 2024 IEEE International Symposium on Antennas and Propagation and INC/USNC-URSI Radio Science Meeting (AP-S/INC-USNC-URSI)*, July 2024, pp. 763–764.

[13] K. L. Wong, S. E. Hong, and W. Y. Li, "Low-Profile Four-Port MIMO Antenna Module Based 16-Port Closely-Spaced 2×2 Module Array for 6G Upper Mid-Band Mobile Devices," *IEEE Access*, vol. 11, pp. 110796–110808, 2023.

[14] K. -L. Wong, Y. -H. Hsu, C. -Y. Lee and W. -Y. Li, "Wideband 4-Port Patch Antenna Module Based Compact 8-Port Two-Module Antenna for 6G Upper Mid-Band 8×4 Device MIMO With Enhanced Spectral Efficiency," *IEEE Access*, vol. 12, pp. 88976–88991, 2024.

[15] K. D. Hong, X. Zhang, H. Y. Weng, L. Zhu, and T. Yuan, "A 2-D Self-Decoupling Method Based on Antenna-Field Redistribution for MIMO Patch Antenna Array," *IEEE Antennas and Wireless Propagation Letters*, vol. 23, no. 3, pp. 940–944, 2024.